

# Assessment of Radar Signal Attenuation Caused by the Melting Hydrometeor Layer

Sergey Y. Matrosov

**Abstract**—Attenuation of radar signals by melting hydrometeors is studied using modeling approaches and comparisons of simulated and observed results. In spite that the melting layer in precipitating systems is usually relatively thin ( $\sim 500$  m), this attenuation can be substantial at X-band frequencies for low elevation angles and at millimeter-wavelength frequencies that are used by the U.S. Department of Energy's Atmospheric Radiation Measurement Program and CloudSat radars operating at vertical/nadir incidence. Melting layer attenuation is stronger than the attenuation in the resultant rain at comparable path lengths and needs to be accounted for in remote sensing methods that use radar reflectivity measurements for retrieving cloud and precipitation parameters if the radar beam penetrates this layer. The choice of the mixing rule for calculating dielectric constants of melting hydrometeors determines, to a significant degree, the magnitude of the modeled attenuation values. A relatively simple Wiener mixing rule provides results that are consistent with melting layer reflectivity enhancements and attenuation estimates from the X-band radar observations. The total melting layer attenuation  $A$  is related to the resultant rain rate  $R$  in an approximately linear manner at X- and  $K_a$ -band frequencies, whereas at W-band, the melting layer attenuation increase with rain rate is slower due to strong non-Rayleigh scattering effects. Typical  $A$ - $R$  relations are suggested, and the variability of these relations is discussed. This paper is mostly concerned with precipitating systems associated with snowflakes that are unrimed or only slightly rimed above the freezing level, as indicated by relatively low values of vertical Doppler velocities.

**Index Terms**—Atmospheric measurements, attenuation, dielectric bodies, meteorological radar, scattering.

## I. INTRODUCTION

THE AREA of the enhanced radar reflectivity factor (hereafter, just reflectivity)  $Z_e$  in a layer of melting hydrometeors, known as a radar bright band (BB), is a feature that is commonly observed in radar measurements of precipitation at traditional radar frequencies. The main cause for this enhancement is a fast increase in dielectric constants of melting particles compared to those of snowflakes in the beginning of the melting process, which leads to higher backscatter cross sections below the freezing level. As melting progresses, the in-

crease in the fall velocity of melting particles, which diminishes their number concentrations, and the decrease in particle sizes results in a rapid reduction of reflectivity in the lower part of the melting layer. At centimeter-wavelengths, reflectivity of rainfall is usually substantially smaller than reflectivity observed at the maximum enhancement in the melting layer. For ground-based millimeter-wavelength radars due to non-Rayleigh scattering effects, BB reflectivity features are progressively less pronounced as the frequency increases [1].

Although attenuation of radar signals in the melting layer has been largely ignored for traditional precipitation radar frequencies such as those at S- (wavelength  $\lambda \sim 10$ – $11$  cm) and C-band ( $\lambda \sim 5$  cm), it might be appreciable at X-band ( $\lambda \sim 3$  cm) and higher radar frequencies (e.g., [2] and [3]). Since the introduction of polarimetric algorithms to correct attenuation in rain (e.g., [4]–[6]), transportable X-band radars are increasingly used for precipitation measurements in the areas that lack adequate coverage by longer wavelength weather surveillance radars (e.g., [7]). Operating scanning polarimetric X-band radars in mountainous areas often results in relatively long propagation path lengths in the melting layer [8], so assessments of the BB signal losses are essential for quantitative precipitation estimations (QPEs).

Vertically pointing millimeter-wavelength radars operating at  $K_a$  ( $\lambda \sim 8$  mm) and W- ( $\lambda \sim 3$  mm) bands, such as the ones used by the U.S. Department of Energy's Atmospheric Radiation Measurement (ARM) Program, were originally intended for remote sensing of nonprecipitating clouds. In spite of significant attenuation in rain, which increases with frequency, these radar signals, however, often penetrate the whole layer of stratiform rain, and can observe ice cloud sections aloft. Ice cloud retrieval methods typically use absolute reflectivity measurements, so for the characterization of atmospheric hydrometeors in the whole vertical column above the ground-based sites, it is necessary to account for attenuation of radar signals in the melting layer and rain. Although there are approaches that can handle rain attenuation of millimeter-wavelength radar signals in rain (e.g., [9]), attenuation of radar signals at these wavelengths in the melting layer remains largely uncharacterized.

Accounting for attenuation of W-band signals in the melting layer is also essential for interpreting measurements of the spaceborne CloudSat radar [10], which shows a potential to be a valuable tool for rainfall studies. This accounting is important for rainfall retrieval techniques that use surface reference signals and/or estimates of absolute reflectivity in the rain layer. CloudSat retrievals of rainfall based on gradient reflectivity measurements [11] are, however, immune to attenuation in the melting layer.

Manuscript received June 5, 2007; revised July 31, 2007. This work was supported in part by the Office of Science, U.S. Department of Energy under Grant DE-FG02-05ER63954, by the National Aeronautics and Space Administration CloudSat project under Grant NNX07AQ82G, and by the National Oceanic and Atmospheric Administration Hydrometeorological Testbed project.

The author is with the Cooperative Institute for Research in Environmental Sciences, University of Colorado, Boulder, CO 80309 USA, and also with the Earth System Research Laboratory, National Oceanic and Atmospheric Administration, Boulder, CO 80305 USA (e-mail: sergey.matrosov@noaa.gov).

Digital Object Identifier 10.1109/TGRS.2008.915757

This paper presents assessments of attenuation of radar signals in the melting layer at the radar frequencies where this attenuation might be rather substantial (e.g., for X-band slant beam measurements, and for millimeter-wavelength radar measurements at any beam elevation), and it is important that it is accounted for in different remote sensing methods such as retrievals of ice parts of precipitating systems with ground-based millimeter-wavelength radars or vertical profile of reflectivity (VPR) corrections with X-band scanning radars. These assessments use descriptions of the dielectric constants of melting particles and melting layer models that are in general agreement with reflectivity BB observations.

## II. THEORETICAL CONSIDERATIONS

### A. Microphysical and Meteorological Model Assumptions

Most melting layer models developed for radar applications (e.g., [12]–[14]) assume no collision coalescence and breakup processes as a result of melting. According to these assumptions, adopted also in this paper, one snowflake of the size  $D_s$  above the freezing level melts into one raindrop of the size  $D_r$  below the BB. The vertical flux of the hydrometeor number concentrations is preserved throughout the melting layer. Thus, we have

$$n_s(D_s)V_s(D_s) = n_m(D_m)V_m(D_m) = n_r(D_r)V_r(D_r) \quad (1)$$

where  $n_s$ ,  $n_m$ , and  $n_r$  are concentrations of snowflakes above the freezing level, melting hydrometeors in the melting layer, and raindrops below BB, respectively, and  $V_s$ ,  $V_m$ , and  $V_r$  are their fall velocities. The equal-volume spherical diameters of snowflakes  $D_s$  and melting hydrometeors  $D_m$  are related to the raindrop diameter  $D_r$  as

$$D_s = D_r(\rho_w/\rho_s)^{1/3} = D_m(\rho_m/\rho_s)^{1/3} \quad (2)$$

where  $\rho_s$ ,  $\rho_m$ , and  $\rho_w$  are bulk densities of snowflakes, melting hydrometeors, and water, correspondingly.

Changes of bulk densities of aggregate ice particles with size usually are described using a power law:  $\rho_s \sim D_s^{-p}$ . For smaller particles, the bulk density is approximately proportional to the reciprocal of the particle size (i.e.,  $p \approx 1$ , e.g., [15]). For larger snowflakes, the rate of density decrease with size is smaller. In their classical study, Magono and Nacamura [16] indicate that, for mostly “dry” snow, the density of falling snowflakes changes (on average) approximately from  $0.03 \text{ g}\cdot\text{cm}^{-3}$  at  $D_s \sim 1\text{--}2 \text{ mm}$  to about  $0.01 \text{ g}\cdot\text{cm}^{-3}$  at  $D_s \sim 2\text{--}2.5 \text{ cm}$  ( $p \approx 0.5$ ). This range of changing densities was assumed for modeling studies here. Uncertainties in modeling results due to the density assumptions were then estimated.

Fall velocities of snowflakes with sizes greater than 1–2 mm also change very little with size, as indicated in a study [17]. It was further assumed that, immediately above the freezing level,  $V_s = 1.5 \text{ m}\cdot\text{s}^{-1}$ . This fall velocity value is consistent with measurements of Doppler velocities performed with vertically pointing radar beams during the Hydrometeorological Testbed (HMT-06) experiments conducted in California [8]. It is also consistent with limited snowflake riming, as follows from the

results in [18]. The fall velocities of raindrops as a function of size were adopted from [19]. It was assumed that the volume fraction of water in a melting particle linearly changes with height between these two levels.

The distance fallen by a melting particle until it is completely turned to a raindrop is size dependent [20]. This distance was calculated using the model from [21], assuming a  $6^\circ \cdot \text{km}^{-1}$  temperature gradient and 100% relative humidity in the melting layer. The fall velocities of melting particles were assumed to depend on the volume fraction of water, as predicted by Mitra *et al.* [21]. Fall velocities were also corrected for the height changes in the air density.

To allow consideration of the effects of particle nonsphericity, the hydrometeors were modeled as oblate spheroids randomly oriented with their major dimensions in the horizontal plane as dictated by aerodynamic forcing. The aspect ratio was assumed to be 0.6, which corresponds to a value that best explains observed dual-wavelength radar measurements in ice regions of precipitating systems [22]. The aspect ratio of melting particles was assumed to vary from 0.6 to the values that are characteristic of raindrops, as specified by an empirical relation in [23].

### B. Dielectric Properties of Melting Particles

To a significant degree, dielectric constants of melting particles govern the BB reflectivity enhancement and attenuation coefficients in the melting layer. Melting hydrometeors are usually modeled either as uniform mixtures of air, solid ice, and water, or as concentric spheres with different constants for the inner core and the coat. The constants for mixtures  $\varepsilon_m$  are typically calculated using a certain mixing rule. Two of the most popular mixing rules used in radar meteorology are represented by the approaches of Maxwell Garnet (MG) [24] and Wiener [25]. The Wiener approach provides for  $\varepsilon_m$  as

$$(\varepsilon_m - 1)(\varepsilon_m + u)^{-1} = P_w(\varepsilon_w - 1)(\varepsilon_w + u)^{-1} + P_i(\varepsilon_i - 1)(\varepsilon_i + u)^{-1} + P_a(\varepsilon_a - 1)(\varepsilon_a + u)^{-1} \quad (3)$$

where  $P_w$ ,  $P_i$ ,  $P_a$  and  $\varepsilon_w$ ,  $\varepsilon_i$ ,  $\varepsilon_a$  are the volume fractions and dielectric constants of water, solid ice, and air, correspondingly (note that  $P_w + P_i + P_a = 1$ ), and  $u$  is a dimensionless factor which increases with the mixture density  $\rho_m$  from about 2 (for  $\rho_m < 0.08 \text{ g}\cdot\text{cm}^{-3}$ ) to  $\infty$  (for  $\rho_m = 1 \text{ g}\cdot\text{cm}^{-3}$ ), as shown in [26].

The MG approach is generally more complex. For a simpler two-component mix, when spherical inclusions with  $\varepsilon = \varepsilon_{\text{inc}}$  are embedded in a matrix with  $\varepsilon = \varepsilon_{\text{mat}}$ , this approach provides [27]

$$\varepsilon_m = \varepsilon_{\text{mat}}(1 + 2cF)(1 - cF)^{-1} \quad (4)$$

where

$$F = (\varepsilon_{\text{inc}} - \varepsilon_{\text{mat}})(\varepsilon_{\text{inc}} + 2\varepsilon_{\text{mat}})^{-1} \quad (5)$$

and  $c$  is the volume fraction of inclusions. The solutions for a two-component mix are different (except for  $c = 0$  or 1), depending on which of the two components is considered a

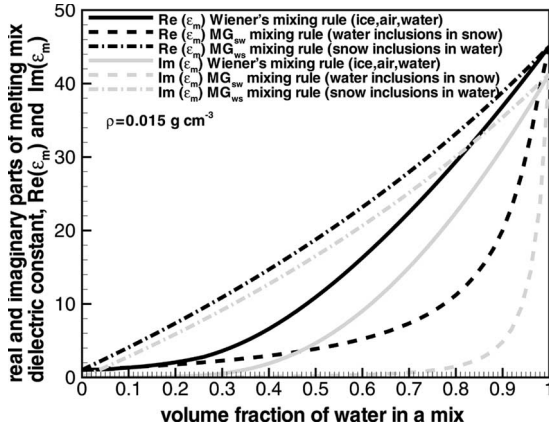


Fig. 1. Dielectric constants of melting particles at X-band calculated as a function of the volume fraction of water using different mixing rules.

matrix and which is treated as inclusions. Note that both the Wiener approach and the MG formula for a two-component mix of solid ice inclusions in an air matrix provide the same solution for the “dry” low-density snow (i.e.,  $u = 2$ ) dielectric constant  $\varepsilon_s$ . Thus, we have

$$(\varepsilon_s - 1)(\varepsilon_s + 2)^{-1} = (\rho_s/\rho_i)(\varepsilon_i - 1)(\varepsilon_i + 2)^{-1} \quad (6)$$

where  $\rho_i$  and  $\varepsilon_i$  are the density and dielectric constant of solid ice, respectively, and it is assumed that  $c = \rho_s/\rho_i$  and  $\varepsilon_a = 1$ . Relation (6) is widely used in radar meteorology (e.g., [28]).

A typical approach of using the MG mixing rule for the three-component mix is to calculate the dielectric constant of the two-component mix and then to consider the resultant dielectric constant as inclusions in the matrix of the third component or as the matrix with the third component inclusions. This generally admits 12 different solutions depending on how the three constituents are ordered [29]. One physically reasonable way is to calculate the dry snow dielectric constant assuming solid ice inclusions in an air matrix and then to calculate dielectric constants of melting hydrometeors as snow inclusions in a water matrix or water inclusions in the snow matrix. An example of dielectric constants of melting particles  $\varepsilon_m$  as calculated using these approaches is shown in Fig. 1 for  $\lambda = 3.2$  cm. Also shown in this figure are the results from Wiener’s formula (3). The dielectric constants of solid ice and water were adopted from [30] and [31], correspondingly.

As can be seen in Fig. 1, the MG rule provides significantly higher dielectric constants for dry snow inclusions in the water matrix mix  $(\varepsilon_m)_{ws}$ , which are defined further as the  $MG_{ws}$  results, compared to the water inclusions in the dry snow matrix mix  $(\varepsilon_m)_{sw}$ . Intuitively, one can suggest that the former mix would be more physically justifiable for larger values of the water fraction  $P_w$ , and the latter one for smaller values of  $P_w$ , so a weighted MG dielectric constant value can be considered as

$$\varepsilon_m = (\varepsilon_m)_{sw}f_s + (\varepsilon_m)_{ws}f_w \quad (7)$$

where  $f_w$  and  $f_s$  are weights ( $f_w + f_s = 1$ ). Since the maximum “packing” for spherical inclusions results in the volume

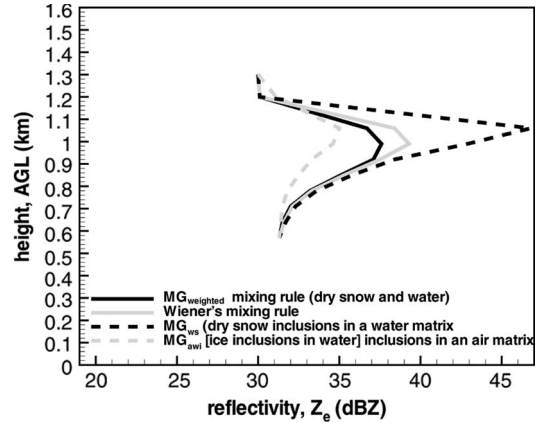


Fig. 2. Modeled profiles of X-band reflectivity for different dielectric constant mixing rules for a  $3\text{-mm} \cdot \text{h}^{-1}$  rain rate. Freezing level height is at 1.2 km AGL.

fractions of inclusions being about 0.63 [27], it is assumed for the MG weighted rule (defined further as  $MG_{weighted}$ ) that

$$f_s = 1 \quad f_w = 0, \quad \text{for } P_w < 0.37 \quad (8a)$$

$$f_w = 1 \quad f_s = 0, \quad \text{for } P_w > 0.63 \quad (8b)$$

and  $f_s$  (and  $f_w$ ) are linearly scaled between 1 and 0 (and between 0 and 1) with respect to  $P_w$  for  $0.37 \leq P_w \leq 0.63$ .

### III. BB REFLECTIVITY ENHANCEMENT

Dielectric constants of melting particles calculated using the model assumptions and different mixing rules mentioned above were used to estimate BB reflectivity enhancements at X-band, as shown in Fig. 2. For presented modeling results, it was assumed that the drop size distributions (DSDs) in the resultant rain below the melting level are described by the approximation of Marshall–Palmer (MP) [32] corresponding to rain rate  $R = 3 \text{ mm} \cdot \text{h}^{-1}$ . The T-matrix method [33] was used to calculate reflectivity and attenuation coefficient values of hydrometeors. Fig. 2 also shows results of modeling of VPRs for the case when the dielectric constants of melting particles were calculated using the MG rule for the ice inclusions in a water matrix mix that were then treated as inclusions in an air matrix (defined further as  $MG_{awi}$  results).

It can be seen in Fig. 2 that  $MG_{awi}$  mixing provides the smallest BB reflectivity enhancement, whereas  $MG_{ws}$  mixing results in an enhancement which is greater by about 12 dB. This is in general agreement with the findings in [34], where the  $MG_{awi}$  and  $MG_{ws}$  mixings (their models 1 and 3) were also considered. Note that their results indicate that the coated particle assumption (a snow core with a water shell) provides X-band BB enhancements similar to those of  $MG_{ws}$  mixing. Modeled profiles obtained using the Wiener and  $MG_{weighted}$  rules are in between the  $MG_{awi}$  and  $MG_{ws}$  result bracket. The relative positions of the Wiener approach BB reflectivity enhancements approximately correspond to those provided by model 5 in [34] which, according to their Figs. 3 and 4, closely approximate observations.

Although the absolute values of reflectivity significantly increase with increasing of rain rate below the melting layer, the BB reflectivity enhancements exhibit relatively little variation

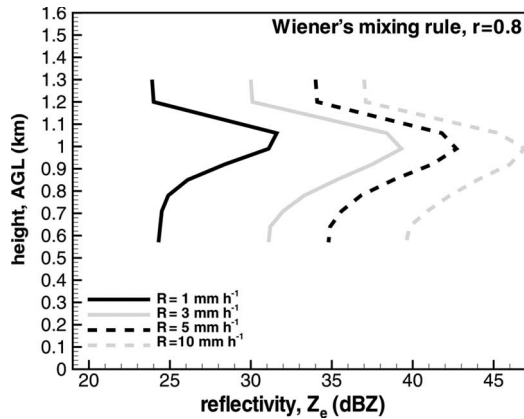


Fig. 3. Modeled profiles of X-band reflectivity for different resultant rain rates. Wiener's mixing rule was used for calculating dielectric constant of melting particles.

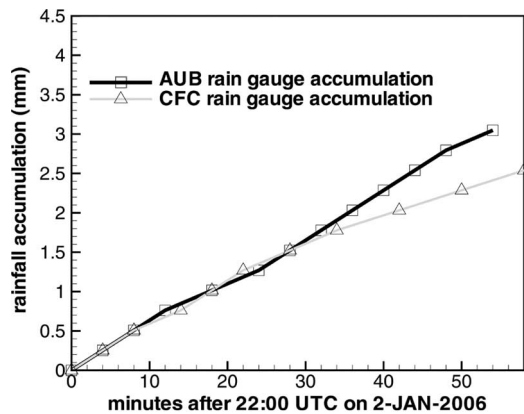


Fig. 4. Rain accumulations at the AUB and CFC sites between 22:00 and 23:00 UTC on January 2, 2006.

as a function  $R$ , as depicted in Fig. 3, which shows BB reflectivity profiles calculated using Wiener's mixing rule for melting hydrometers and MP DSDs. The relative position of the BB maximum shifts downward, and the BB becomes a little thicker with increasing rain rate as the number of larger particles increases with  $R$ , so the melting process takes more time.

#### A. Comparisons With X-Band Radar Measurements

The NOAA Earth System Research Laboratory's X-band scanning polarimetric radar was used in precipitation measurements during the HMT-06 field project held in winter 2005–2006 in northern California [8]. The main operational mode of the radar during precipitation events included low elevation angle sector scans and over the top (i.e., including vertical viewing) range–height indicator (RHI) scans. The RHI scans were used to reconstruct VPRs at different ranges from the radar.

Comparisons of modeled BB profiles of reflectivity with X-band radar measurements indicated that Wiener's mixing rule provided the best agreement between calculated and observed profiles. Some examples of such comparisons for one of the precipitation events observed on January 2, 2006 are given below. The rainfall accumulations as measured by tipping buckets rain gauges at the Auburn (AUB) site, where the radar

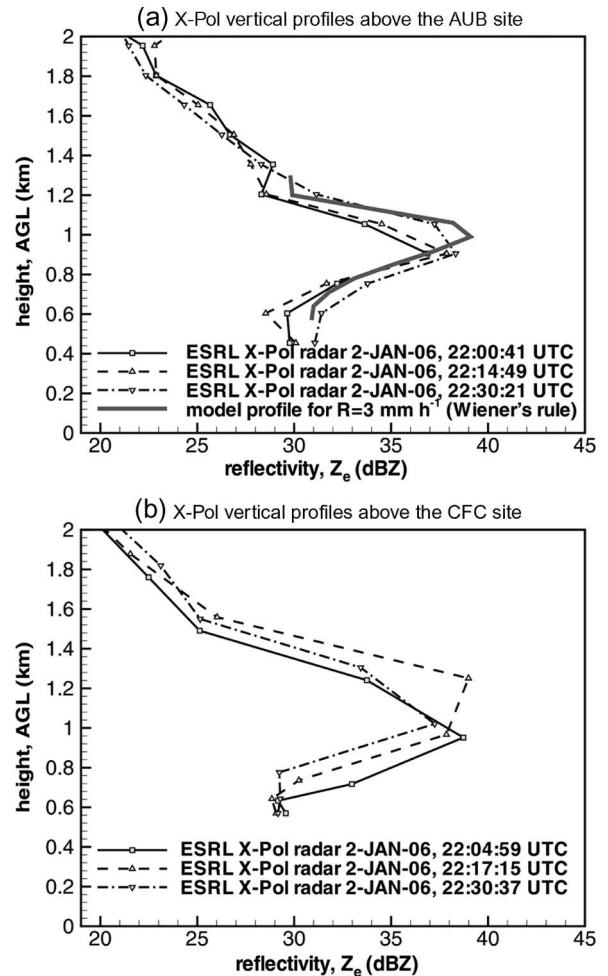


Fig. 5. Observations of vertical profiles of X-band reflectivity in steady rain ( $R \sim 3 \text{ mm} \cdot \text{h}^{-1}$ ) above (a) AUB and (b) CFC sites on January 2, 2006 (22:00–22:30 UTC).

was deployed, and at the Colfax (CFC) ground validation site located at 18.1 km from the radar are shown in Fig. 4 for the period between 22:00 and 23:00 coordinated universal time (UTC). These accumulation results indicate that for the first 30 min during this hour, the rain at the AUB and CFC sites was relatively steady with  $R \approx 3 \text{ mm} \cdot \text{h}^{-1}$ . The height of the  $0^\circ$  isotherm during this time period was at about 1.2 km above ground level (AGL). This relatively uniform period of stratiform rain is convenient for comparing BB measurements with low elevation and vertical radar beams.

Profiles of X-band radar reflectivity at the AUB site measured with a vertically pointing radar beam are shown in Fig. 5(a). These measured profiles changed relatively little during the 30-min time period indicated above. Also shown in Fig. 5(a) is the modeled reflectivity profile calculated for  $R = 3 \text{ mm} \cdot \text{h}^{-1}$  using Wiener's mixing rule with assumptions stated in Section II. The agreement between the theoretical and measured BB reflectivity enhancements is fairly good, although the observed reflectivity maxima are positioned a little lower above the ground compared to the modeled data. The BB thickness of observed data is a little greater than for the theoretical profile, although some differences can be expected due to relatively crude spatial resolution of the X-band radar ( $\sim 150 \text{ m}$ ).

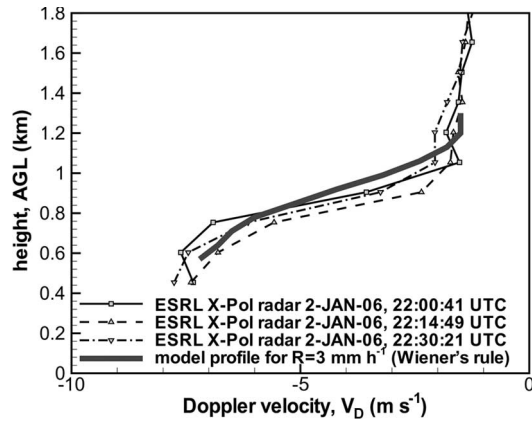


Fig. 6. Comparison of the modeled and observed X-band Doppler velocity profiles) above AUB site and CFC site on January 2, 2006 (22:00–22:30 UTC).

Fig. 5(b) shows vertical profiles of measured X-band radar reflectivity above the AUB site that were reconstructed from the RHI measurements directed along the line connecting the AUB radar site and the CFC ground validation site. As in the case with the AUB profiles [Fig. 5(a)], measured CFC profiles show rather little variation during the period of steady rain. Although the BB appears thicker, in part due to beam broadening effects (the NOAA X-band radar beamwidth is about  $0.85^\circ$ ), overall, there is a good correspondence between BB features at AUB and CFC.

The observed reflectivities shown in Fig. 5(b) were corrected for attenuation in rain at a path length between the AUB and CFC sites using the differential phase shift measurements, as discussed in [7]. Since no corrections for the BB attenuation were introduced, the difference in reflectivities above both these sites at a height of about 1.5 km AGL (i.e., where the beam is out of the melting layer for both AUB and CFC sites) is expected to be mostly due to the two-way attenuation in the melting layer, as the reflectivity in the rain regions is approximately the same for both sites ( $\sim 30$  dBZ). Judging from Fig. 5(a) and (b), this difference, however, is rather small and can be approximately estimated as about 1.5–2 dB, or so. Moreover, this difference is expected to decrease with height AGL because the radar samples higher areas above the CFC site using higher elevation radar beams, thus reducing the path length in the melting layer.

For the same times as in Fig. 5(a), Fig. 6 shows measurements of vertical Doppler velocity  $V_D$  above the AUB site. Superimposed on these measurements are also modeled profiles of  $V_D$  obtained using the Wiener's mixing rule for dielectric constants of melting particles. The agreement between modeled and measured profiles is fairly good except maybe in the nearest vicinity of the freezing level. The profiles that are shown in Figs. 5 and 6 are characteristics of those observed during the HMT-06 field experiment.

#### IV. MODEL ESTIMATIONS OF ATTENUATION IN THE MELTING LAYER

Comparisons of modeled and measured X-band reflectivity profiles in the melting layer indicate that the relatively simple Wiener mixing rule provides modeling results for VPRs that are

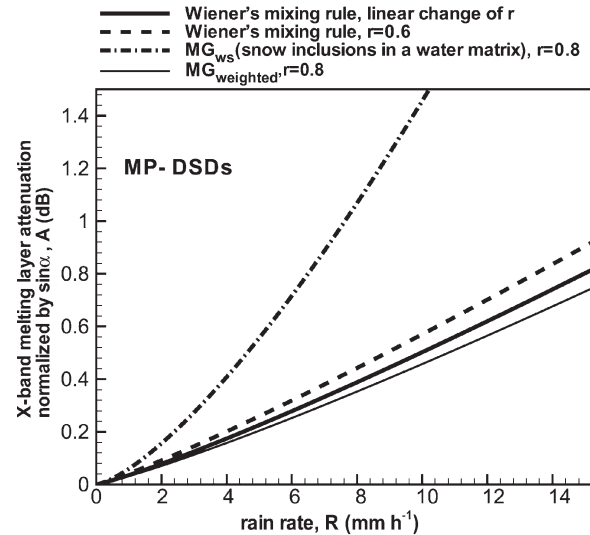


Fig. 7. Attenuation of X-band radar signals in the melting layer as a function of resultant MP rain rate for different mixing rules of dielectric constants and particle aspect ratios  $r$ .

in general agreement with observations. It might be expected that this rule would provide suitable results also for the melting layer attenuation estimates. In this section, the melting layer model assumptions discussed in Section II were used to simulate estimates of attenuation of the radar signals of different frequencies. It should be admitted, however, that the consistency of the simulation results with reflectivity measurements does not necessarily guarantee the model appropriateness for attenuation assessment, so the intermodel variability also needs to be estimated.

##### A. Assessment of X-Band Radar Signal Attenuation

Model calculations of the two-way attenuation of X-band radar signals ( $\lambda = 3.2$  cm) in the melting layer  $A$  as a function of resultant rain rate are shown in Fig. 7. Since this attenuation is particularly important for the low radar elevation angle  $\alpha$  measurements, which are typical for quantitative precipitation measurements, the calculations were performed for values of  $\alpha$  in the range between  $1^\circ$  and  $10^\circ$ , and an average value of  $A$ , which is normalized by the factor  $\sin(\alpha)$ , is depicted. The horizontal polarization of the radar signals was further assumed for the slant beam geometry.

It can be seen in Fig. 7 that the Wiener and  $MG_{\text{weighted}}$  mixing rules provide similar results for the melting layer attenuation, as they do for the BB reflectivity enhancement (Fig. 2). Assuming that aspect ratios of melting particles are  $r = 0.6$  throughout the whole melting layer causes relatively minor differences ( $\sim 10\%$ – $12\%$ ). The attenuation values for the  $MG_{\text{ws}}$  mixing rule (i.e., snow inclusions in a water matrix) are significantly larger (a factor of 2–2.5 or so in the decibel scale for  $1 \text{ mm} \cdot \text{h}^{-1} < R < 6 \text{ mm} \cdot \text{h}^{-1}$ ) than those for the other mixing rules shown. Judging from Fig. 2, the dielectric constants predicted by the  $MG_{\text{ws}}$  rule also result in the highest BB reflectivity enhancements, which are not usually observed in the experimental data. Changes in other model assumptions (e.g., varying the density of “dry” snow by 20% and varying the fall velocity of dry snowflakes in a range  $1.3$ – $1.5 \text{ m} \cdot \text{s}^{-1}$ )

result in relatively minor ( $< 15\%$ ) variations in the results presented in Fig. 7. The corresponding best fit power law for the total attenuation in the melting layer at X-band, assuming Wiener's dielectric constants for melting particles, is  $A(\text{dB}) = 0.048R^{1.05}$ , where the resultant rain rate  $R$  is  $\text{mm} \cdot \text{h}^{-1}$ .

The Wiener mixing rule results for the melting layer attenuation at  $R = 3 \text{ mm} \cdot \text{h}^{-1}$  are in general agreement with observations shown in Fig. 5. In these observations, the radar beam cleared the melting level above the CFC site at  $\alpha \approx 4.5^\circ$ , and the model results at this elevation angle provide  $A \approx 2 \text{ dB}$ . Note that given relatively small attenuation values, one can regard this comparison as a consistency check between modeling and observation results but not a strict validation.

Overall, for Wiener's mixing rule assumption, the melting layer attenuation of X-band radar signals at beam elevations  $\alpha \geq 3^\circ$  and rain rates  $R < 4 - 5 \text{ mm} \cdot \text{h}^{-1}$  can be expected to be generally within 4 dB or so. Such rain rates were typical for colder events in HMT-06 when BB effects were present in the X-band radar QPE coverage area. In a VPR correction approach suggested for this experiment [8], it is currently assumed that, on average, the rain region reflectivities exceed reflectivities in the snow region just above the freezing level by about 2 dB, and this value does not change with rain rate. Judging from the results given above, this is likely to be an overall appropriate assumption for typical BB conditions at HMT-06. Using lower elevation angles and observing higher average rain rates in the presence of BB would likely require more detailed modeling of VPR.

As seen in Fig. 7, the relationship between the melting layer attenuation at X-band and the resultant rain rate for the  $MG_{\text{weighed}}$  and Wiener's mixing rules is close to linear. The use of experimental DSDs measured at the ground by an impact Joss-Waldvogel disdrometer (JWD) instead of the model MP DSD data results (not shown) in  $A-R$  relations similar to those in Fig. 7. The data scatter due to variability in experimental DSD details is typically within 15%. The small data scatter and the general linearity of  $A-R$  relations probably mean that both  $A$  and  $R$  are proportional to similar moments of the particle size distribution.

It is instructive also to compare theoretical and observed assessments of melting layer attenuation values for higher rain rates, although such rain rates were not very typical for most of the events observed during HMT-06. Fig. 8 shows a vertical profile of measured X-band reflectivity over the CFC site obtained from the RHI radar scan at 13:14 UTC on December 31, 2005. It was a relatively warm event with a freezing level height of about 2.1 km AGL, and the rain rate  $R \approx 10 \text{ mm} \cdot \text{h}^{-1}$  at around this time as estimated from the JWD measurements at the CFC site. The reflectivity profiles for the vertical beam at the AUB radar site were unavailable due to saturation of the radar receivers at short ranges in rain of such intensity.

The radar beam in Fig. 8 is completely out of the melting layer at a height of about 2.4 km AGL, which corresponds to an elevation angle  $\alpha \approx 7.6^\circ$ , as observed from the AUB radar site. As before, the attenuation of radar signals in rain (but not in the melting layer) was accounted for using the differential phase shift measurements. A difference between the rain layer reflectivity and the reflectivity at  $\sim 2.4 \text{ km AGL}$  is expected

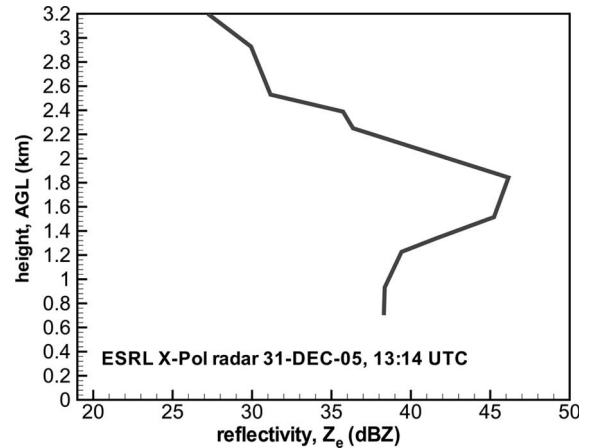


Fig. 8. Vertical profile of X-band reflectivity measurements observed at 13:10 UTC on December 31, 2005 above the CFC site as reconstructed from an RHI scan.  $R \approx 10 \text{ mm} \cdot \text{h}^{-1}$ , and the attenuation correction in rain was applied to the data.

to be mostly due to the two-way attenuation in the melting layer. This is because the nonattenuated snow reflectivity just above the melting layer and the nonattenuated reflectivity of the resultant rain just below the melting layer are very similar at X-band, as shown in Fig. 3. The observed difference of about 4–5 dB between these reflectivities is in fair agreement with an estimate in Fig. 7, which suggests a melting layer attenuation at  $R \approx 10 \text{ mm} \cdot \text{h}^{-1}$  of about 4 dB (for the Wiener mixing rule assumption) after accounting for a  $1/\sin(7.6^\circ)$  factor. Although this comparison between the model and observation data (as well as the comparison for the January 2 event in Fig. 5) cannot be regarded as a strict validation attempt, it shows that measurements are consistent with modeling results.

### B. Assessment of $K_a$ - and W-Band Radar Signal Attenuation

Millimeter-wavelength cloud radars (MMCRs) that operate at  $K_a$ - and W-bands are mostly used for hydrometeor profiling with a beam pointing either vertically for the ground-based radars (e.g., [35]) or in the nadir direction for airborne and spaceborne radars (e.g., [10]). Quite often, these radars (particularly,  $K_a$ -band radars) can “see” through the melting layer of precipitating systems. Thus, it is most appropriate to estimate the melting layer attenuation at these frequencies for the vertical direction.

The same assumptions, as for the X-band modeling above, were applied to the millimeter-wavelength frequencies. The  $K_a$ -band melting layer attenuation values  $A$  shown in Fig. 9 were obtained for the ARM radar wavelength ( $\lambda = 0.87 \text{ cm}$ ). It can be seen that a general linearity of  $A$  with respect to the resultant rain rate still holds. For the Wiener's dielectric constant assumption, the best fit at  $K_a$ -band is  $A$  (in decibels) =  $0.66R^{1.1}$ . Attenuation of  $K_a$ -band radar signals in the melting layer is much stronger than for X-band frequencies. As was shown in [9], the  $K_a$ -band attenuation coefficient in rain  $\alpha$  is also approximately proportional to rainfall rate  $R$  [ $\alpha$  (in decibels per kilometer)  $\approx 0.28R$  (in millimeters per hour)]. Thus, the above modeling results indicate that at  $K_a$ -band for typical rainfall rates between 1 and  $10 \text{ mm} \cdot \text{h}^{-1}$ , the melting layer attenuation is about a factor of 2.5–3 larger than

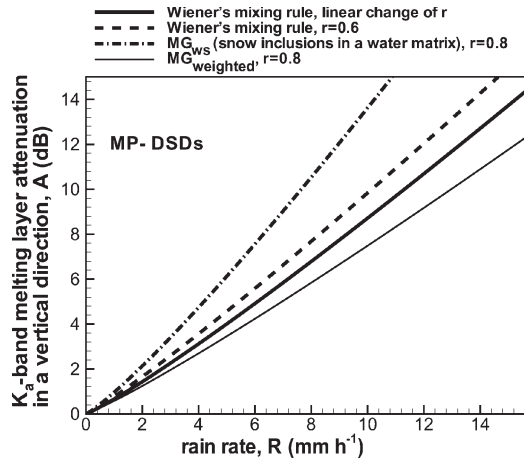


Fig. 9. Attenuation of  $K_a$ -band radar signals in the melting layer at vertical incidence as a function of resultant MP rain rate for different mixing rules of dielectric constants and particle aspect ratios  $r$ .

attenuation in the resultant rain with the same layer thickness. Thus, fact is in general agreement with results from [36].

Although the relative difference between the  $MG_{weighted}$  and Wiener mixing rule results at  $K_a$ -band is very similar to that of X-band, the  $K_a$ -band  $MG_{ws}$  mixing rule data are much closer to the results of other mixing rules shown in Fig. 9. The influence of the particle aspect ratio and “dry” snow density assumptions remains quite modest (less than 15% when aspect ratio is changed from 0.8 to 0.6, or the snow density changed by 20%), although melting particles with a larger degree of nonsphericity attenuate radar signals stronger. Since a relation between  $A$  and  $R$  at  $K_a$ -band (as at X-band) is relatively close to linear, it is likely that the DSD variability of the resultant rain is not a significant factor in changes of melting layer attenuation at  $K_a$ -band.

A typical example of measurements in a stratiform rain taken by a vertically pointing ARM  $K_a$ -band radar is shown in Fig. 10. The rainfall rate corresponding to this event was about  $5 \text{ mm} \cdot \text{h}^{-1}$  [9]. Although radar reflectivity signals are in saturation between 0 and 1 km AGL (note that an additional 23-dB attenuator is installed in ARM radars when they operate in precipitation mode), there is an obvious attenuation in rain layer between 1 and 2.6 km AGL. The freezing level height for this event was at 3.1 km AGL. Superimposed on measurement data are results of BB reflectivity modeling with and without accounting for the melting layer attenuation (attenuation in rain is accounted for in both cases). It can be seen that the melting layer attenuation significantly reduces BB reflectivity enhancement. The modeling results when this attenuation is accounted for are in better agreement with observed data. Note that reflectivity values in snow just above the melting layer are significantly less than those in rain just below it. This is due to a combination of the dielectric constant and non-Rayleigh scattering effects. The melting layer attenuation increases the difference between these reflectivity values by about 4 dB for this case. It can also be seen that the modeled vertical profile of  $V_D$  [Fig. 10(b)] is in good agreement with MMCR vertical Doppler velocity measurements.

W-band frequencies are the highest used routinely for radar remote sensing, and radar signals at these frequencies ex-

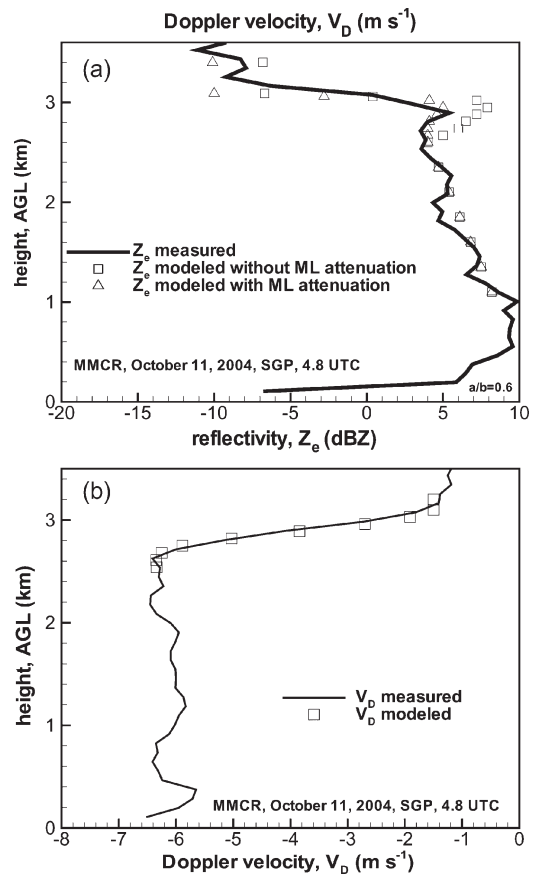


Fig. 10. Comparisons of modeled and measured (a)  $K_a$ -band reflectivity and (b) Doppler velocity profiles in a stratiform rain with  $R \approx 5 \text{ mm} \cdot \text{h}^{-1}$ .

perience the strongest atmospheric attenuation. Although the gaseous absorption at W-band is fairly well known and can be accounted for in a relatively straightforward way (e.g., [10]), the hydrometeor attenuation needs to be understood better to successfully use the W-band radars for precipitation measurements. Model assessments of the melting layer attenuation at a representative W-band frequency of 94 GHz (i.e., the CloudSat radar frequency) are shown in Fig. 11.

One feature of W-band is that the variability of attenuation due to the choice of the dielectric constant mixing rule is substantially smaller compared to longer radar wavelengths. The difference between the Wiener rule and the  $MG_{ws}$  rule results is typically within 20%, compared to a factor of about 2.5 for X-band and a factor of about 1.5 for  $K_a$ -band (in the decibel scale). The melting layer attenuation  $A$  increases with the resultant rain rate  $R$  at a slower rate than for lower frequencies, and the deviation from the linear relation is more significant. For 94 GHz, the best power law fit for Wiener's mixing rule is:  $A(\text{dB}) = 2.6R^{0.87}$ . The strong non-Rayleigh scattering effects are likely to be the main factor responsible for this slower rate of increase at W-band.

Modeling with HMT experimental DSDs (not shown) indicates that, at W-band, DSD details matter more than at X- and  $K_a$ -bands. The variability in the melting layer attenuation due to DSD can be on the order of variability due to different mixing rules that are shown in Fig. 11. It should be mentioned that while attenuation is a major factor for changes in W-band

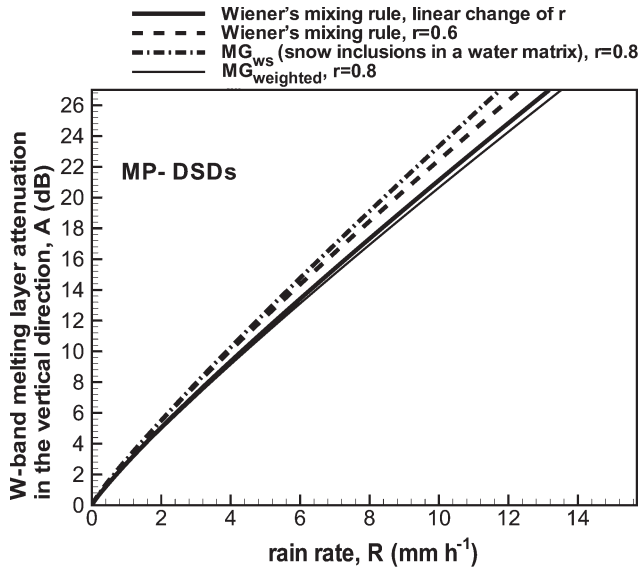


Fig. 11. Same as in Fig. 9 but for W-band.

radar signal in the melting layer, other factors such as multiple scattering (for spaceborne radars) can also significantly impact measured reflectivities.

## V. SUMMARY AND CONCLUSION

Attenuation caused by hydrometeors in the melting layer notably exceeds that of the resultant rain at the same path lengths. In some practical cases such as X-band radar measurements at low elevation angles and millimeter-wavelength radar measurements at any beam elevation, the attenuation of radar signals in the melting layer is often significant. It needs to be accounted for in cloud and precipitation remote sensing methods that rely on the estimates of absolute values of radar reflectivity at the ranges beyond the BB.

Model representations of the melting layer were used in this paper to assess the magnitude of attenuation in the melting layer as a function of the intensity of the rain that results from the melting process. The assumption for the dielectric constants of the melting hydrometeors significantly influences the magnitude of the BB attenuation at X-band, but is progressively less important as the frequency increases. A relatively simple Wiener mixing rule representing melting particles as a homogeneous mixture of water, air, and solid ice was shown to provide a fair agreement with the BB reflectivity enhancements and estimates of the melting layer attenuations observed with X-band radar measurements during the HMT-06 field experiment.

The relations between the attenuation in the melting  $A$  and the resultant rain rate  $R$  are close to be linear at  $K_a$ - and X-band frequencies. Depending on the melting hydrometeor aspect ratios, the Wiener mixing rule for dielectric constants predicts about a 0.25–0.3-dB melting layer X-band attenuation at  $R \sim 5 \text{ mm} \cdot \text{h}^{-1}$  (normalized for a vertical incidence), whereas the MG rule for snow inclusions in a water matrix results in about a factor of 2.5 larger (in the decibel scale) attenuation. The Wiener rule results and the results obtained with the weighted MG rule, however, were found to be more consistent with reflectivity BB observations made using the NOAA X-band

scanning polarimetric radar. The variability of melting layer attenuation values with respect to the assumptions of dry snow density (as soon as these densities remain in a range that is characteristic of snow with a small degree of riming) and aspect ratios of melting particles were found to be relatively minor compared to the assumption of the dielectric constant mixing rule.

At  $K_a$ -band, the attenuation in the melting layer, according to Wiener's mixing rule, is a factor of about 2.5–3 higher than in the resultant rain of the same layer thickness. It reaches a value of about 8–9 dB for  $R \sim 10 \text{ mm} \cdot \text{h}^{-1}$ , whereas the  $\text{MG}_{\text{ws}}$  results are about 50%–60% higher (in the decibel scale). The Wiener results, however, are consistent with experimental data from [36], where it is indicated that attenuation in wet/watery snow, which is a proxy for the melting layer, at  $K_a$ -band is about two to three times stronger than attenuation in rain of the same liquid equivalent intensity. These results for ( $R \approx 4 \text{ mm} \cdot \text{h}^{-1}$ ) are about 50% higher (in the decibel scale) than those reported in [2] for a frequency of 30 GHz. The frequency difference between 34.6 and 30 GHz, however, can account for some of the discrepancy in melting layer attenuation estimates. The BB modeling results for  $K_a$ -band were consistent with MMCR observations in stratiform rain.

At W-band, in part due to strong non-Rayleigh scattering effects, the dielectric mixing rule choice matters less than for lower frequencies. The difference between the rain and melting layer attenuations is also smaller compared to other wavelengths while the resultant rain DSD variations are more important. The melting layer attenuation at W-band increases with  $R$  at a slower rate compared to X- and  $K_a$ -bands.

The microphysical and dynamical model of the melting layer used in this paper (Section II-A) results in a melting layer geometrical thickness which is approximately 500 m at  $3 \text{ mm} \cdot \text{h}^{-1}$  and slightly increases for larger values of  $R$  (see Fig. 3). Such geometrical thicknesses are generally consistent with most radar observations (e.g., those made during the HMT-06 field project). For higher BB thicknesses, which are occasionally observed experimentally, the assessment results presented in this paper would, probably, underestimate attenuation in the melting layer. It can be expected, however, that the total melting layer attenuation can be approximately scaled with BB geometrical thickness.

## REFERENCES

- [1] K. Sassen, J. R. Campbell, J. Zhu, P. Kollias, M. Shupe, and C. Williams, "Lidar and triple-wavelength Doppler radar measurements of the melting layer: A revised model for dark- and brightband phenomena," *J. Appl. Meteorol.*, vol. 44, no. 3, pp. 301–312, 2005.
- [2] W. Klaassen, "Attenuation and reflection of radio waves by a melting layer of precipitation," *Proc. Inst. Electr. Eng.—H*, vol. 137, no. 1, pp. 39–44, Feb. 1990.
- [3] A. Bellon, I. Zawadzki, and F. Fabry, "Measurements of melting layer attenuation at X-band frequencies," *Radio Sci.*, vol. 32, no. 3, pp. 943–955, 1997.
- [4] S. Y. Matrosov, K. A. Clark, A. Tokay, and B. E. Martner, "X-band polarimetric radar measurements of rainfall," *J. Appl. Meteorol.*, vol. 41, no. 9, pp. 941–952, Sep. 2002.
- [5] M. N. Anagnostou, E. N. Anagnostou, and J. Vivekanandan, "Correction for rain path specific and differential attenuation of X-band dual-polarization observations," *IEEE Trans. Geosci. Remote Sens.*, vol. 44, no. 9, pp. 2470–2480, Sep. 2006.

- [6] S.-G. Park, M. Maki, K. Iwanami, V. N. Bringi, and V. Chandrasekar, "Correction of radar reflectivity and differential reflectivity for rain attenuation at X-band—Part II: Evaluation and application," *J. Atmos. Ocean. Technol.*, vol. 22, no. 11, pp. 1633–1655, 2005.
- [7] S. Y. Matrosov, D. E. Kingsmill, B. E. Martner, and F. M. Ralph, "The utility of X-band polarimetric radar for quantitative estimates of rainfall parameters," *J. Hydrometeorol.*, vol. 6, no. 3, pp. 248–262, Jun. 2005.
- [8] S. Y. Matrosov, K. A. Clark, and D. E. Kingsmill, "A polarimetric radar approach to identify rain, melting layer and snow regions for applying corrections to vertical profiles of reflectivity," *J. Appl. Meteorol. Clim.*, vol. 46, no. 2, pp. 154–166, Feb. 2007.
- [9] S. Y. Matrosov, P. T. May, and M. D. Shupe, "Rainfall profiling using atmospheric radiation measurement program vertically pointing 8-mm wavelength radars," *J. Atmos. Ocean. Technol.*, vol. 23, no. 11, pp. 1478–1491, Nov. 2006.
- [10] G. L. Stephens, "The CloudSat mission and the A-train," *Bull. Amer. Meteorol. Soc.*, vol. 83, no. 12, pp. 1771–1790, Dec. 2002.
- [11] S. Y. Matrosov, "Potential for attenuation-based estimations of rainfall rate from CloudSat," *Geophys. Res. Lett.*, vol. 34, no. 5, L05 817, 2007. DOI:10.1029/2006GL029161.
- [12] W. Szyrmer and I. Zawadzki, "Modeling of the melting layer—Part I: Dynamics and microphysics," *J. Atmos. Sci.*, vol. 56, no. 20, pp. 3573–3592, Oct. 1999.
- [13] W. S. Olson, P. Bauer, N. F. Viltard, D. E. Johnson, W.-K. Tao, R. Meneghini, and L. Liao, "A melting layer model for passive/active microwave remote sensing applications—Part I: Model formulation and comparisons with observations," *J. Appl. Meteorol.*, vol. 40, no. 7, pp. 1145–1163, Jul. 2001.
- [14] I. Zawadzki, W. Szyrmer, C. Bell, and F. Fabry, "Modeling of the melting layer—Part III: The density effect," *J. Atmos. Sci.*, vol. 62, no. 10, pp. 3705–3723, Oct. 2005.
- [15] P. R. A. Brown and P. N. Francis, "Improved measurements of the ice water content in cirrus using a total-water probe," *J. Atmos. Ocean. Technol.*, vol. 12, no. 4, pp. 410–414, Apr. 1995.
- [16] C. Magono and T. Nakamura, "Aerodynamic studies of falling snowflakes," *J. Meteorol. Soc. Jpn.*, vol. 43, no. 3, pp. 139–147, 1965.
- [17] D. L. Mitchell and A. J. Heymsfield, "Refinements in the treatment of ice particle terminal velocities, highlighting aggregates," *J. Atmos. Sci.*, vol. 62, no. 5, pp. 1637–1644, May 2005.
- [18] L. Mosimann, "An improved method for determining the degree of snow crystal riming by vertical Doppler radar," *Atmos. Res.*, vol. 37, no. 4, pp. 305–323, Aug. 1995.
- [19] R. Gunn and G. D. Kinzer, "The terminal velocity of fall for water drops in stagnant air," *J. Meteorol.*, vol. 6, pp. 243–248, 1949.
- [20] K. Sassen, S. Matrosov, and J. Campbell, "CloudSat spaceborne 94 GHz radar bright bands in the melting layer: An attenuation-driven upside-down lidar analog," *Geophys. Res. Lett.*, vol. 34, no. 16, L16 818, 2007. DOI:10.1029/2007GL030291.
- [21] S. K. Mitra, O. Vohl, M. Ahr, and H. R. Pruppacher, "A wind tunnel and theoretical study of the melting behavior of atmospheric ice particles—IV: Experiment and theory for snow flakes," *J. Atmos. Sci.*, vol. 47, no. 5, pp. 584–591, Mar. 1990.
- [22] S. Y. Matrosov, A. J. Heymsfield, and Z. Wang, "Dual-frequency radar ratio of non-spherical atmospheric hydrometeors," *Geophys. Res. Lett.*, vol. 34, L05 817, 2005. DOI:10.1029/2005GL023210.
- [23] E. A. Brandes, G. Zhang, and J. Vivekanandan, "Corrigendum," *J. Appl. Meteorol.*, vol. 44, no. 11, p. 186.
- [24] J. C. Maxwell Garnett, "Colours in metal glasses and in metallic films," *Philos. Trans. R. Soc. London A, Math. Phys. Sci.*, vol. 203, pp. 385–420, 1904.
- [25] O. Wiener, "Zur Theorie der Refraktionskonstanten," *Berichte über die Verhandlungen der Königlich Sächsischen Gesellschaft der Wissenschaften zu Leipzig Math. Phys. Klasse*, 1910. Bd 62, Heft 5.
- [26] T. Ihara, Y. Furuhashi, and K. Tohma, "Measurement of depolarization due to snowfall at 34.5 GHz," *Trans. IECE Jpn.*, vol. 65, no. 1, pp. 16–22, 1982.
- [27] V. N. Bringi and V. Chandrasekar, *Polarimetric Doppler Weather Radar*. Cambridge, U.K.: Cambridge Univ. Press, 2001.
- [28] L. J. Battan, *Radar Observations of the Atmosphere*. Chicago, IL: Univ. Chicago Press, 1973.
- [29] R. Meneghini and L. Liao, "Effective dielectric constants of mixed-phase hydrometeors," *J. Atmos. Ocean. Technol.*, vol. 17, no. 5, pp. 628–640, May 2000.
- [30] S. G. Warren, "Optical constants of ice from ultraviolet to the microwave," *Appl. Opt.*, vol. 23, no. 8, pp. 1206–1225, 1984.
- [31] V. I. Rozenberg, *Scattering and Extinction of Electromagnetic Waves by Atmospheric Particles*. Leningrad, Russia: Gidrometeoizdat, 1972.
- [32] J. S. Marshall and W. M. Palmer, "The distribution of raindrops with size," *J. Meteorol.*, vol. 5, no. 4, pp. 165–166, Aug. 1948.
- [33] P. Barber and C. Yeh, "Scattering of electromagnetic waves by arbitrarily shaped dielectric bodies," *Appl. Opt.*, vol. 14, no. 12, pp. 2864–2872, 1975.
- [34] F. Fabry and W. Szyrmer, "Modeling of the melting layer—Part II: Electromagnetic," *J. Atmos. Sci.*, vol. 56, no. 20, pp. 3593–3600, Oct. 1999.
- [35] P. Kollias and B. Albrecht, "Why the melting layer radar reflectivity is not bright at 94 GHz," *Geophys. Res. Lett.*, vol. 32, no. 24, L24 818, 2005. DOI:10.1029/2005GL024074.
- [36] T. Oguchi, "Electromagnetic wave propagation and scattering in rain and other hydrometeors," *Proc. IEEE*, vol. 71, no. 9, pp. 1029–1078, Sep. 1983.



**Sergey Y. Matrosov** received the Ph.D. degree in geophysics from the Main Geophysical Observatory, St. Petersburg, Russia, in 1985.

He is currently a Research Scientist with the Cooperative Institute for Research in Environmental Sciences, University of Colorado, Boulder. He is also affiliated with the National Oceanic and Atmospheric Administration's Earth System Research Laboratory, Boulder. His areas of expertise include active and passive atmospheric remote sensing, radar polarimetrics, and electromagnetic propagation. His current

research interests include developing and applying algorithms for retrieving atmospheric hydrometeor parameters from ground-based and spaceborne remote sensors.

Dr. Matrosov is a member of the American Geophysical Union and the American Meteorological Society.